Evaluating luminescence based voltage images of silicon solar cells

M. Glatthaar,[1,a)] J. Haunschild,[1,2] R. Zeidler,[1] M. Demant,[1,2] J. Greulich,[1,2] B. Michl,[1] W. Warta,[1] S. Rein,[1] and R. Preu[1]
[1]*Fraunhofer Institute for Solar Energy Systems ISE, Heidenhofstr. 2, 79110 Freiburg, Germany*
[2]*Material Research Center, University of Freiburg, Stefan-Meier-Str. 21, 79104 Freiburg, Germany*

(Received 23 March 2010; accepted 29 April 2010; published online 2 July 2010)

In this paper we give a mathematical derivation of how luminescence images of silicon solar cells can be calibrated to local junction voltage. We compare two different models to extract spatially resolved physical cell parameters from voltage images. The first model is the terminal connected diode model, where each pixel is regarded as a diode with a certain dark saturation current, which is connected via a series resistance with the terminal. This model is frequently used to evaluate measurement data of several measurement techniques with respect to local series resistance. The second model is the interconnected diode model, where the diode on one pixel is connected with the neighbor diodes via a sheet resistance. For each model parameter at least one image is required for a coupled determination of the parameters. We elaborate how also the voltage calibration can be added as an unknown parameter into the models, and how the resulting system of equations can be solved analytically. Finally the application of the models and the different ways of voltage calibration are compared experimentally. © *2010 American Institute of Physics*.
[doi:10.1063/1.3443438]

I. INTRODUCTION

Electroluminescence and photoluminescence (EL/PL) imaging are fast and nondestructive methods for spatially resolved characterization of silicon solar cells. In the last years many new methods have been published to evaluate luminescence images quantitatively.[1–11] One possibility to determine spatially resolved the effective charge carrier diffusion length $L_{eff}(x,y)$ directly from the luminescence intensity $I(x,y)$ was developed by Fuyuki *et al.*[1] For this, excitation conditions are chosen such that lateral differences of the junction voltage are expected to be small. This approach has the disadvantage that it only holds for L_{eff} much smaller than the cell thickness. In general L_{eff} depends on bulk lifetime, back surface recombination velocity, and emitter saturation current density. All those parameters affect $I(x,y)$ differently. In addition the doping level and the surface texture strongly influence $I(x,y)$. A determination of $L_{eff}(x,y)$ can therefore be very difficult and requires a detailed previous knowledge of the sample. The influence of different parameters can partly be separated by a spectral analysis of the luminescence radiation.[3,6,8,12] Disadvantages of this approach are large experimental errors either due to a poor signal to noise ratio, when analyzing the short wavelength part of the spectrum or due to wavelength dependent blurring, when analyzing the long wavelength part of the spectrum. In this paper we will discuss another approach in detail: luminescence images can be calibrated to junction voltage.[2] In this paper we will give a stringent mathematical derivation for this calibration.

When a certain device model is applied to voltage calibrated images its parameters can be determined. We will give a systematic overview of how device parameters can be determined from voltage images for two different device models. We will see which possibilities there are beyond what has already been published.

II. THEORY

A. Voltage calibration of luminescence images

For the moment we follow the description of a solar cell as a quasi-one-dimensional system with spatial coordinate z. The contribution of the solar cell's base to the luminescence intensity I as a function of the excess charge carrier distribution $n(z)$ is given by the integral

$$I = \int_0^d w(z)n(z)dz, \tag{1}$$

with the base thickness d and the probability $w(z)$ that an electron recombines radiatively and the emitted photon escapes from the cell. Under low injection conditions $n(z)$ satisfies the differential equation

$$\frac{n(z)}{\tau} - Dn''(z) = G(z), \tag{2}$$

with the bulk lifetime τ, the diffusion constant D, and the generation rate $G(z)$. At the pn-junction ($z=0$) we have the boundary condition

$$n(0) = \frac{n_i^2}{N_A}\exp\left(\frac{V}{V_T}\right), \tag{3a}$$

with the intrinsic charge carrier density n_i, the acceptor density N_A, the junction voltage V, and the thermal voltage V_T. At the back we have the boundary condition

[a)]Electronic mail: markus.glatthaar@ise.fraunhofer.de.

$$n(d) = -n'(d)D/S_b, \tag{3b}$$

with the back surface recombination velocity S_b. For $G(z)=0$ Eq. (2) is a homogeneous linear differential equation. From Eq. (3a) and the linearity of Eq. (2) then follows that $n(z)$ scales exponentially with the junction voltage for all z. We can split the solution of the homogeneous Eq. (2) into a spatially dependent and a voltage dependent factor

$$n_{\mathrm{hom}}(z) = n_0(z)\left[\exp\left(\frac{V}{V_T}\right) - 1\right] \approx n_0(z)\exp\left(\frac{V}{V_T}\right). \tag{4}$$

Setting Eq. (4) into Eq. (1) shows that for the homogeneous Eq. (2), which holds for EL, also the luminescence intensity I depends exponentially on V.

For PL the inhomogeneous Eq. (2) has to be solved. We split the solution $n_{inh}(z)$ into the homogeneous solution $n_{hom}(z)$ and a particular solution $n_p(z)$ that satisfies the boundary condition $n(0)=0$

$$n_{inh}(z) = n_0(z)\exp\left(\frac{V}{V_T}\right) + n_p(z). \tag{5}$$

Please note that for the boundary condition chosen for the particular solution $n_p(z)$ is proportional to $G(z)$. We set Eq. (5) into Eq. (1) and obtain

$$I = \exp\left(\frac{V}{V_T}\right)\int_0^d w(z)n_0(z)dz + \int_0^d w(z)n_p(z)dz. \tag{6}$$

Equation (6) shows that the luminescence intensity I can be written as the sum of one part depending exponentially on the junction voltage V and one part that is proportional to the generation $G(z)$ and the illumination intensity I_L, respectively. It can easily be seen that for strong enough generation and small or even negative junction voltage the left summand of Eq. (6) related to electrically injected charge carriers becomes negligible compared to the right summand related to optically generated charge carriers. The PL intensity $I(x,y)$ for a position (x,y) can be written as

$$I(x,y) = C(x,y)\exp\left(\frac{V(x,y)}{V_T}\right) + B(x,y)I_L, \tag{7}$$

with the calibration constant $C(x,y)$, depending on the integral of the left summand in Eq. (6) and the background $B(x,y)$ depending on the right summand in Eq. (6).

An explicit voltage calibration can be done in the following way:

To determine $B(x,y)$ one image $I_B(x,y)$ is taken at short circuit or if necessary at negative bias voltage and at known illumination intensity $I_{L,B}$. We obtain

$$B(x,y) = I_B(x,y)/I_{L,B}. \tag{8}$$

At open circuit and sufficiently low illumination intensity $I_{L,C}$, where lateral voltage gradients are negligible, a second image $I_C(x,y)$ is taken to determine $C(x,y)$. From the assumption that $V(x,y)$ is equal to the measured open circuit voltage V_C we obtain

$$C(x,y) = [I_C(x,y) - B(x,y)I_{L,C}]/\exp(V_C/V_T). \tag{9}$$

With knowledge of $C(x,y)$ and $B(x,y)$ Eq. (7) allows determining $V(x,y)$ for an arbitrary image $I(x,y)$

$$V(x,y) = V_T \log\left(\frac{I(x,y) - B(x,y)I_L}{C(x,y)}\right). \tag{10}$$

Taking the emitter into account is analogous and will not change the final result Eq. (10). The contribution of the space charge region to the luminescence intensity is negligible. It does not influence the voltage calibration either, as long as boundary condition Eq. (3a) still holds, which generally is the case as the space charge region is thin enough not to limit charge carrier transport.

The voltage calibration described here is not much different to the procedure described by Trupke *et al.* However the insight from the theoretical derivation we have presented allows determining the illumination dependent contribution to the signal from only one short circuit image e.g., at an illumination equivalent of one sun. For Trupke's calibration an additional short circuit image at low illumination intensity was needed, almost doubling the total data acquisition time.

B. Evaluating voltage images

To determine the local physical properties of a solar cell from voltage images requires a certain model with parameters that reflect these properties.

1. Model 1: Terminal connected diodes

A simple approach is to describe a large area solar cell by many diodes with an ideality factor of $n=1$. Each diode is connected via a series resistance to the terminal. The voltage drop between the terminal and a position (x,y) is given by Ohm's law and the one-diode-model

$$V_{appl} - V(x,y) = R(x,y)\{j_0(x,y)\exp[V(x,y)/V_T] - j_p\}, \tag{11}$$

with the voltage applied at the terminal V_{appl} and photocurrent density j_p, which is assumed to be laterally constant and equal to the short circuit current density of the device. The model parameters to be determined are the series resistance $R(x,y)$ between a position (x,y) and the terminal, and the dark saturation current density $j_0(x,y)$. The two parameters cannot be determined by applying Eq. (11) to a single voltage image without further information. One option is to determine $j_0(x,y)$ by the approximation of Fuyuki *et al.*[1] They assume that the bulk diffusion length L scales reciprocally with the EL intensity at low applied voltage. This approximation only holds for L much smaller than the cell thickness. The contribution of the emitter dark saturation current j_{0E} has to be either negligible or to be laterally constant and ulterior known.

Another option is to use the information of more than one voltage image.

$V(x,y)$ occurs in Eq. (11) linearly and in an exponential expression. This guarantees that for a number of voltage images taken at different applied voltages or photocurrents we obtain a set of linearly independent equations. This allows a

coupled determination of $j_0(x,y)$ and $R(x,y)$ from two voltage images. It can easily be seen at Eq. (11) that only PL with $j_p \neq 0$ allows to separate the two parameters, while with EL ($j_p=0$) only the product j_0R can be determined. In principle also a shunt or a second diode term can be added to Eq. (11). For each new parameter an additional image is required. However according to our experience this will fail, as the underlying model with the local diodes connected via a series resistance to the terminal is a quite rough approximation itself. Deficits of this model will erroneously occur in the parameters describing the local diode properties.

Coupled voltage calibration. Kampwerth *et al.*[5] and Breitenstein *et al.*[10] have demonstrated two different methods to determine $R(x,y)$, where no explicit voltage calibration was necessary. This helps to lower the data acquisition time as no low illumination (PL) or low applied voltage (EL) image is needed. On the other hand both methods require time consuming numerical algorithms to calculate a full image. For Kampwerth's method a rather large series of images is needed and the information of $j_0(x,y)$ is eliminated. Breitenstein has to rely on Fuyuki's approximation[1] for $j_0(x,y)$ as EL is used.

We present here an analytical solution for a coupled voltage calibration and determination of $R(x,y)$ and $j_0(x,y)$, by setting Eq. (10) into Eq. (11). We determine $B(x,y)$ from a short circuit image. With $I^*(x,y)=I(x,y)-B(x,y)I_L$ we obtain

$$\underbrace{V_{appl}-V_T \ln I^*(x,y)}_{b_i} = \underbrace{-V_T \ln C(x,y)}_{s_1} \underbrace{-j_p}_{A_{i,2}} \underbrace{R(x,y)}_{s_2} + \underbrace{I^*(x,y)}_{A_{i,3}} \underbrace{\frac{R(x,y)j_0(x,y)}{C(x,y)}}_{s_3}. \tag{12}$$

With the substitutions indicated by the braces in Eq. (12) we obtain from a set of three images for each pixel a linear equation system $b_i=\Sigma A_{i,j}s_j$, that can easily be solved for s_i. Here i denotes the number of the respective image with its excitation conditions.

Finally we obtain $C(x,y)=\exp(-s_1/V_T)$, $R(x,y)=s_2$, $j_0(x,y)=s_3C(x,y)/R(x,y)$. Interestingly it is not sufficient to take all PL images with the same illumination intensity. Otherwise $A_{i,2}s_2$ and $-V_T \ln C(x,y)$ would reduce to the constant part of the system of equations and it would not be possible to separate $C(x,y)$ and $R(x,y)$, and finally $j_0(x,y)$.

2. Model 2: Interconnected diodes

In a sound model of a large area solar cell we have to describe a cell element at a position (x,y) by a local current density $j(x,y)$ which flows through the device and a lateral current $\mathbf{I}(x,y)$ transported by the emitter with the sheet resistance $\rho(x,y)$ toward the metal grid on the front side. Combining Ohm's law Eq. (13a) and the continuity equation Eq. (13b) we obtain

$$\nabla V(x,y) = \rho(x,y)\mathbf{I}(x,y), \tag{13a}$$

$$\nabla \cdot \mathbf{I}(x,y) = j(x,y), \tag{13b}$$

$$\rightarrow \nabla^2 V(x,y) = \rho(x,y)j(x,y) + \nabla\rho(x,y)\mathbf{I}(x,y) \approx \rho(x,y)j(x,y). \tag{13c}$$

The approximation in Eq. (13c) holds for a short circuit current smaller than 35 $\mathrm{mA/cm^2}$ and a gradient of the emitter sheet resistance smaller than 10 Ω/mm. So, some care has to be taken when using this model for nonstandard cell concepts.

Applying a one-diode model we obtain

$$\nabla^2 V(x,y) = \rho(x,y)\{j_0(x,y)\exp[V(x,y)/V_T]-j_p\}. \tag{14}$$

For a constant previously known emitter sheet resistance we already used Eq. (13c) to determine $j_0(x,y)$ from a voltage calibrated EL image. With two voltage calibrated PL images also a coupled determination of $j_0(x,y)$ and $\rho(x,y)$ is straight forward.

Coupled voltage calibration. When we set Eq. (10) into Eq. (13c) for a coupled voltage calibration we obtain

$$\underbrace{V_T\nabla^2 \ln I^*(x,y)}_{b_i} = \underbrace{V_T\nabla^2 \ln C(x,y)}_{s_i} \underbrace{-j_p}_{A_{i,2}} \underbrace{\rho}_{s_2} \underbrace{+I^*}_{A_{i,3}} \underbrace{\frac{\rho j_0}{C(x,y)}}_{s_3}. \tag{15}$$

Mathematically the solution of the system of equations obtained from applying Eq. (15) to a series of three PL images is found in the same way as described above, when using the substitutions indicated by the braces. Although, a difference is that with s_1 we only obtain the Laplacian of the calibration constant C_i.

III. EXPERIMENTAL

The images are acquired with a thermoelectrically cooled Silicon charge coupled device. The solar cell is placed on a temperature stabilized copper chuck at 25 °C, which also contacts the cell backside electrically. The busbars on the front side are contacted with nine spring loaded current conducting tips each and one additional voltage probe tip. The solar cell is illuminated with expanded laser light at 790 nm. The laser light is blocked by a long pass filter stack in front of the camera lens.

For *independent voltage calibration* we take one image at short circuit and an illumination equivalent to AM 1.5 (1.0 suns) with respect to the short circuit current density to determine $B(x,y)$ from Eq. (8). The image to determine $C(x,y)$ from Eq. (9) we take at open circuit and 0.2 suns. To determine $j_0(x,y)$ and $R(x,y)$ using *model 1* Eq. (11) is applied to one voltage calibrated image taken at 1.0 suns and a terminal voltage where 25% of short circuit current is extracted and one image where 75% is extracted. The idea is that for both images the current extraction paths are similar. Furthermore the local voltages should be different enough to allow the separation of the two parameters. To determine $j_0(x,y)$ and $\rho(x,y)$ using *model 2* Eq. (14) is applied to the same voltage calibrated images.

For *coupled voltage calibration using model 1* we use the same image series. $B(x,y)$ is determined as described above. The three images applied to Eq. (12) are the open

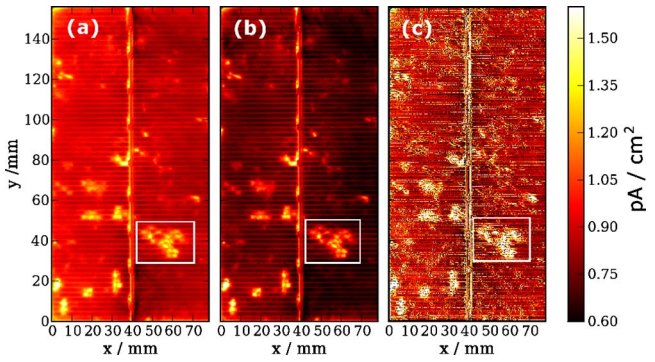

FIG. 1. (Color online) Dark saturation current images obtained by (a) independent voltage calibration using model 1, (b) coupled voltage calibration using model 1, and (c) independent voltage calibration using model 2.

circuit image at 0.2 suns and the two images at 1.0 suns with 25% and 75% of the short circuit current being extracted.

IV. RESULTS AND DISCUSSION

In Fig. 1 we compare three j_0-images. One image obtained by independent [Fig. 1(a)], one by coupled voltage calibration [Fig. 1(b)] using model 1, and one image obtained from independent voltage calibration using model 2 [Fig. 1(c)]. The three images show very similar structures. But the histogram in Fig. 2 shows, that the absolute values differ. We obtain significantly lower values for $j_0(x,y)$ with the coupled voltage calibration compared to independent voltage calibration using model 1. A detailed analysis reveals that for coupled voltage calibration the results depend on the excitation conditions at which the images are taken. A certain dependence is also observed for independent voltage calibration but is not as strong. We have to keep in mind that in particular model 1 is a considerable simplification. Hence, it is not surprising, that the determined parameters depend on the excitation conditions. More important is the fact that obviously with independent and with coupled voltage calibration a reliable separation of different physical information, i.e., dark saturation current and series resistance is achieved.

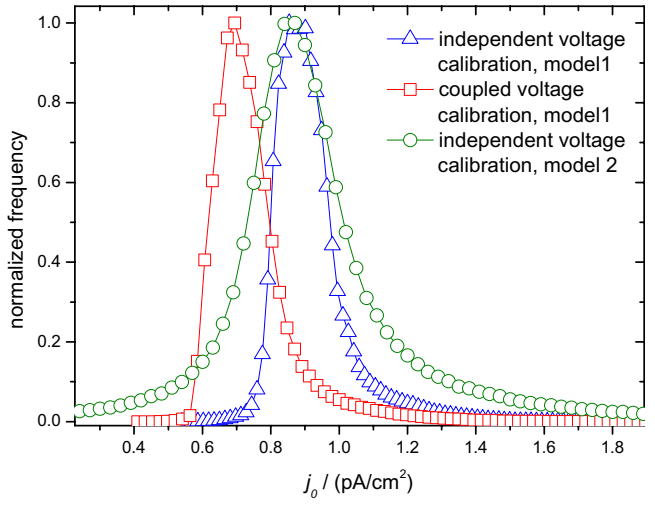

FIG. 2. (Color online) Histograms of the different dark saturation current images shown in Fig. 1.

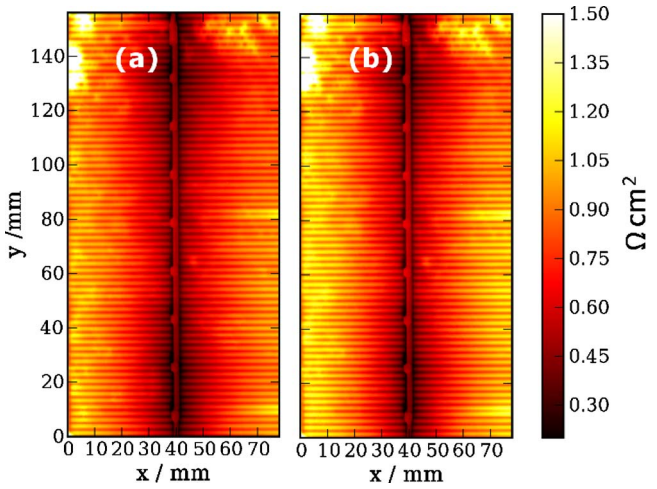

FIG. 3. (Color online) Series resistance images obtained using model 1 with (a) independent voltage calibration and (b) with coupled voltage calibration.

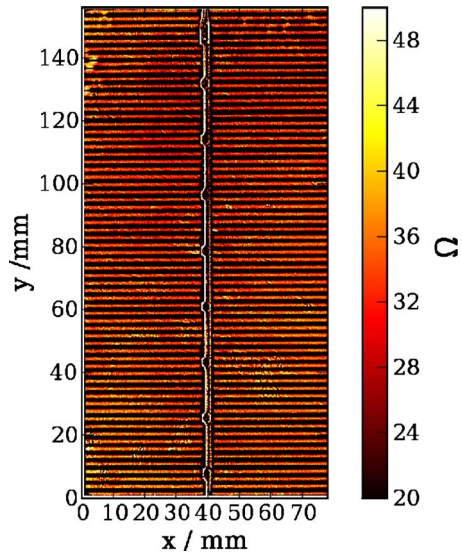

FIG. 4. (Color online) Sheet resistance image obtained using model 2 with independent voltage calibration.

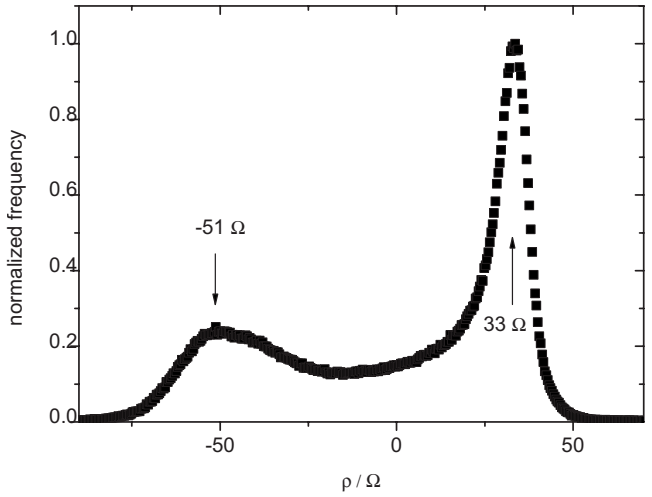

FIG. 5. Histogram of the sheet resistance image (Fig. 4). The peak at −51 Ω is related to metal grid. The peak at 33 Ω is related to the sheet resistance of the emitter.

The series resistance images are also quantitatively very similar for both ways of voltage calibration, as can be seen in Fig. 3.

The average values for $j_0(x,y)$ obtained by independent voltage calibration with model 1 and with model 2 are almost the same. However, the value spread is higher using model 2. As can be seen in Figs. 1(a) and 1(c) this is not only due to more noise. Also the areas with high crystal defect density (exemplarily marked by the white rectangle) show higher values using model 2 compared to model 1. We attribute this to the neglect of interaction between neighbor areas in model 1, which becomes manifest in a blurring of the calculated j_0-images. In a formerly published EL-based method to calculate j_0-images for known constant sheet resistance using model 2 the obtained values have been a factor of 2–3 lower than expected.[7,11] Interestingly this is not the case for coupled determination of $j_0(x,y)$ and $\rho(x,y)$ with PL. Even the strong artifacts at the position of the front side grid vanish in the j_0-image. Instead the artifacts at the grid and the too low values occur in the related ρ-image (Fig. 4). In the histogram of the ρ-image (Fig. 5) we observe a peak at −51 Ω related to the grid artifact and a peak at 33 Ω related to the emitter sheet resistance. This value is a factor of 2 lower than expected for the applied emitter. To get an idea of the reason we have a look at the explicit solution of the equation system derived from Eq. (14). The indices 1 and 2 denote the respective voltage image. For $j_0(x,y)$ we obtain

$$j_0(x,y) = j_p \frac{\nabla^2 V_2(x,y) - \nabla^2 V_1(x,y)}{\nabla^2 V_1(x,y)\exp[V_2(x,y)/V_T] - \nabla^2 V_2(x,y)\exp[V_1(x,y)/V_T]}. \tag{16a}$$

For $\rho(x,y)$ we obtain

$$\rho_i = \frac{1}{j_p} \frac{\nabla^2 V_1(x,y)\exp[V_2(x,y)/V_T] - \nabla^2 V_2(x,y)\exp[V_1(x,y)/V_T]}{\exp[V_1(x,y)/V_T] - \exp[V_2(x,y)/V_T]}. \tag{16b}$$

We see that in case the Laplacian is miscalculated by a constant factor this factor reduces in the fraction of Eq. (16a). It does not in Eq. (16b) as the Laplacian only occurs in the enumerator. Such a constant factor might be caused by a blurring of the voltage images.[11] The artifact at the position of the grid is caused by anisotropy of the sheet resistance. Along the grid we have a much lower sheet resistance than perpendicular to it. In addition we assumed that j_p at the grid was the same as at the blank emitter, which is not true.

V. CONCLUSIONS

We gave a stringent theoretical derivation for the voltage calibration of luminescence images, showing that in principle only injection dependence of charge carrier recombination can cause erroneous calibration. For standard multicrystalline solar cells at open circuit under up to 1.0 suns we usually are still in low injection conditions. So we expect the errors to be small. We have derived that a short circuit image at lowered illumination intensity is not necessary for the voltage calibration. This leads to a significant reduction in the total data acquisition time.

To extract physical cell parameters from voltage calibrated images we investigated two different models such as: the simple terminal connected diode model (model 1) and the more sophisticated interconnected diode model (model 2).

Applying model 1, the physical information is successfully separated into a series resistance and a dark saturation current image. We demonstrated that just as the two model parameters can be determined from two voltage calibrated images, the voltage calibration factor $C(x,y)$, and the two model parameters can be determined analytically from three different images. This has the potential advantage that in principle the images can be taken at higher charge carrier injection levels again reducing the data acquisition time.[10]

With model 2 the sheet resistance and the dark saturation current are determined. Unfortunately the resulting sheet resistance is about a factor of 2 lower than expected. We think that the reason is an erroneous calculation of the Laplacian due to blurring of the voltage images. Further investigations will show if a deblurring can solve this problem. Another disadvantage using this model is the sensitivity of the Laplacian to noise, which leads to increased data acquisition times.

[1] T. Fuyuki, H. Kondo, T. Yamazaki, Y. Takahashi, and Y. Uraoka, Appl. Phys. Lett. **86**, 262108 (2005).
[2] T. Trupke, E. Pink, R. A. Bardos, and M. D. Abbott, Appl. Phys. Lett. **90**, 093506 (2007).
[3] P. Würfel, T. Trupke, T. Puzzer, E. Schäffer, W. Warta, and S. W. Glunz, J. Appl. Phys. **101**, 123110 (2007).
[4] D. Hinken, K. Ramspeck, K. Bothe, B. Fischer, and R. Brendel, Appl. Phys. Lett. **91**, 182104 (2007).
[5] H. Kampwerth, T. Trupke, J. W. Weber, and Y. Augarten, Appl. Phys. Lett. **93**, 202102 (2008).
[6] T. Kirchartz, A. Helbig, and U. Rau, Sol. Energy Mater. Sol. Cells **92**, 1621 (2008).
[7] M. Glatthaar, J. Giesecke, M. Kasemann, J. Haunschild, M. The, W. Warta, and S. Rein, J. Appl. Phys. **105**, 113110 (2009).
[8] J. A. Giesecke, M. Kasemann, and W. Warta, J. Appl. Phys. **106**, 014907 (2009).
[9] J. Haunschild, M. Glatthaar, M. Kasemann, S. Rein, and E. R. Weber, Phys. Status Solidi (RRL) **3**, 227 (2009).
[10] O. Breitenstein, A. Khanna, Y. Augarten, J. Bauer, J.-M. Wagner, and K. Iwig, Phys. Status Solidi (RRL) **4**, 7 (2010).
[11] M. Glatthaar, J. Haunschild, M. Kasemann, J. Giesecke, W. Warta, and S. Rein, Phys. Status Solidi (RRL) **4**, 13 (2010).
[12] U. Rau, Phys. Rev. B **76**, 085303 (2007).